Talanta 238 (2022) 123036

Contents lists available at ScienceDirect

Talanta

journal homepage: www.elsevier.com/locate/talanta

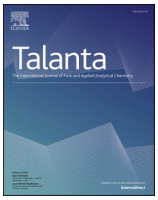

Enhanced voltammetric performance of sensors based on oxidized 2D layered black phosphorus

María A. Tapia [a], Rui Gusmão [b], Clara Pérez-Ràfols [a,c], Xavier Subirats [a], Núria Serrano [a,c,*], Zdeněk Sofer [b,**], José Manuel Díaz-Cruz [a,c]

[a] Department of Chemical Engineering and Analytical Chemistry, University of Barcelona, Martí i Franquès 1-11, 08028, Barcelona, Spain
[b] Department of Inorganic Chemistry, University of Chemistry and Technology Prague, Technicka 5, 166 28, Prague 6, Czech Republic
[c] Water Research Institute (IdRA), University of Barcelona, Martí i Franquès 1-11, 08028, Barcelona, Spain

ARTICLE INFO

Keywords:
2D materials
Black phosphorus
Oxidized black phosphorus
Dopamine
Screen-printed electrodes
Voltammetry

ABSTRACT

The exceptional properties of 2D layered black phosphorus (BP) make it a promising candidate for electrochemical sensing applications and, even though BP is considered unstable and tends to degrade by the presence of oxygen and moisture, its oxidation can be beneficial in some situations. In this work, we present an unequivocal demonstration that the exposition of BP-based working electrodes to normal ambient conditions can indeed be advantageous, leading to an enhancement of voltammetric sensing applications. This point was proved using a BP modified screen-printed carbon electrode (BP-SPCE) for the voltammetric determination of dopamine (DA) as a model target analyte. Oxidized BP-SPCE (up to 35% of P_xO_y at the surface) presented an enhanced analytical performance with a 5-fold and 2-fold increase in sensitivity, as compared to bare-SPCE and non-oxidized BP-SPCE stored in anhydrous atmosphere, respectively. Good detection limit, repeatability, reproducibility, stability, selectivity, and accuracy were also achieved. Overall, the results presented herein display the prominent possibilities of preparing and working with BP based-sensors in normal ambient settings and showcase their implementation under physiological conditions.

1. Introduction

Two-dimensional (2D) materials have been theoretically studied for many years, initially as 'academic materials' that were not believed to be stable [1]. This belief was drastically changed in 2004 with the experimental discovery of graphene [2], which has demonstrated great potential for applications as diverse as catalysis, electronics, energy storage, sensors and biomedicine among others [3]. This success promoted the development of other 2D materials such as layered metal oxides and transition metal dichalcogenides [4]. Particularly interesting is the case of 2D layered materials based on pnictogen elements (i.e. elements of group VA), which arise as promising materials for chemical sensing platforms [5–7]. Among all the 2D layered pnictogens, black phosphorus (BP) is the most recognized and experimentally studied material for electrochemical sensing applications, mainly in the form of gas sensors (e.g., humidity, NO_2, H_2) but also in the development of sensors for the determination of metal ions, biomolecules and drugs [5].

BP is a p-type semiconductor with a layered structure that presents many desirable properties such as an intrinsic and tuneable direct band gap, high carrier mobility, good flexibility and anisotropic electrical conductivity [8–11]. Nevertheless, practical implementation of BP is often hindered by its low stability in ambient conditions. Thus, recent efforts have been devoted to establishing the fundamentals of BP degradation and finding preventive pathways to preserve the material [8]. Regarding the former, there is a general agreement that points out light, temperature, oxygen, and humidity as degradation factors, albeit to a different extent [12–15]. For example, light is a crucial factor in BP deterioration, particularly in the UV region as it facilitates the formation of singlet oxygen and $OH^{\bullet}$ radicals [12]. Then, the role of humidity is less extensive because water molecules only interact with BP once it is already oxidized [15]. On the other hand, research regarding the prevention of BP degradation has primarily focused on preventing BP exposure to ambient conditions. Some of the reported strategies include physical passivation and/or encapsulation [8,9,16–18], capping under

* Corresponding author. Department of Chemical Engineering and Analytical Chemistry, University of Barcelona, Martí i Franquès 1-11, 08028, Barcelona, Spain.
** Corresponding author.
E-mail addresses: nuria.serrano@ub.edu (N. Serrano), zdenek.sofer@vscht.cz (Z. Sofer).

https://doi.org/10.1016/j.talanta.2021.123036
Received 21 August 2021; Received in revised form 29 October 2021; Accepted 3 November 2021
Available online 5 November 2021

other 2D materials [8,9] and surface modification [8,9,19]. Nevertheless, more research is still needed to find protection strategies that provide long-term stability of BP without influencing its intrinsic properties.

Although BP degradation is most often considered as an undesirable event, it has also proven to be beneficial under certain circumstances. For example, phosphorus oxides produced by BP degradation result in a reduced friction force that favors BP lubrication properties [20]. In addition, intrinsic defect states in BP allow its implementation in innovative optoelectronic applications [21], degradation of BP in moist environments can be useful for the determination of humidity [9], and good stability was reported for NO_2 reversible adsorption and desorption in slightly oxidized BP, highlighting its benefits in gas sensing applications [20]. In a similar direction, electrochemical sensing applications could also take advantage of BP degradation. This has indeed been observed for graphene, in which abundant structural defects and functional groups present in reduced graphene oxide (rGO) have been demonstrated to be advantageous for electrochemical applications [22,23]. Thus, it is not unreasonable to test if the same phenomena could also be appropriated for BP.

Therefore, this work explores the possibilities of oxidized BP in electrochemical sensing. For this purpose, a BP modified screen-printed carbon electrode (BP-SPCE) was developed and the effect of BP degradation on its analytical performance was assessed for the voltammetric determination of dopamine (DA) as a model target analyte. DA is a biogenic amine neurotransmitter related to common neurodegenerative diseases such as Alzheimer's, Huntington and Parkinson's disease [24,25]. Oxidation of BP provided an enhanced analytical performance with a 5-fold and 2-fold increase in sensitivity as compared to the bare electrode and the BP sensor stored in anhydrous atmosphere, respectively.

2. Experimental section

2.1. Chemicals and solutions

Red phosphorus (99.999%) and tin (99.999%) were obtained from Strem, Germany. Iodine (resublimed, 99.9%) and chloroform (99.9%) were obtained from Lach-Ner, Czech Republic. Dopamine hydrochloride (purity >98.5%) was purchased from Fluka Chemika (Buchs, Switzerland). Sodium phosphate dibasic dihydrate ($Na_2HPO_4{\cdot}2H_2O$), ascorbic acid, uric acid, salicylic acid, paracetamol, epinephrine hydrochloride and serotonin were purchased from Sigma-Aldrich (St. Louis, MO, USA). Sodium dihydrogen phosphate monohydrate ($NaH_2PO_4{\cdot}H_2O$) was provided by Scharlab (Barcelona, Spain). Ibuprofen was acquired from Acros Organics (Geel, Belgium). All reagents were of analytical grade.

Stock solution of DA was daily prepared in ultrapure water (Milli-Q plus 185 system, Millipore) and diluted to appropriated concentrations. 0.1 M phosphate buffer solution at pH = 7 was used for pH control.

Ultrapure water was employed in all experiments.

2.2. Instrumentation

2.2.1. Characterization

Scanning electron microscopy (SEM) analysis was performed with a field emission gun (FEG) electron source, from Tescan LYRA3 dual-beam microscope, by using a 5 kV electron beam. Energy-dispersive X-ray spectroscopy (EDS) was used for elemental composition and mapping using a 20 mm^2 silicon drift detector (Oxford Instruments) and AZtecEnergy software. The measurements were carried out using a 20 kV electron beam.

High-resolution X-ray photoelectron spectroscopy (XPS) was performed using an ESCAProbeP spectrometer (Omicron Nanotechnology Ltd., Germany) with a monochromatic aluminum X-ray radiation source (1486.7 eV). An electron gun was used to eliminate sample charging during measurement (1–5 V). A wide-scan survey was performed for all elements of each sample with subsequent high-resolution scans of the different core levels P 2p. The XPS survey spectra were analyzed by using CasaXPS software.

Raman spectroscopy measurements were performed on an inVia Raman microscope (Renishaw, England) in backscattering geometry with a Charge Coupled Device (CCD) detector. A diode-pumped solid-state Nd-YAG laser (532 nm, 50 mW) with an applied power of 5% and 50 × magnification objective was used for the measurement, previously calibrated with a silicon reference, which gives a peak position at 520 cm^{-1}.

2.2.2. Electrochemical measurements

Electrochemical measurements were carried out with a μAutolab System Type III (EcoChemie, The Netherlands) coupled to a Metrohm 663 VA Stand (Methohm, Switzerland) and controlled with GPES version 4.9 software (EcoChemie). A three-electrode cell containing the BP-SPCE working electrode prepared from a commercial screen-printed carbon electrode (SPCE) with 4 mm diameter purchased from Metrohm DropSens (Oviedo, Spain) (ref. DRP-110), a platinum auxiliary electrode (Methohm, Switzerland), and an Ag/AgCl/KCl (3 M) (Methohm, Switzerland) as the reference electrode, was used. A flexible cable provided by Metrohm DropSens (ref. CAC) was used to connect the working electrode with the potentiostat. All the potentials are referred to Ag/AgCl/KCl (3 M) reference electrode.

A Crison micropH 2000 (Barcelona, Spain) calibrated with standard solutions of pH 4 and 7 was utilized for pH measurements.

2.3. Experimental procedures

2.3.1. BP preparation

BP was synthesized by direct conversion of red phosphorus using SnI_4/Sn as a mineralizing agent. 2 g of red phosphorus were placed in a quartz ampoule together with 30 mg of SnI_4 and 60 mg of Sn, melted and sealed under high vacuum. The sealed ampoule was placed horizontally in a muffle furnace, being heated for 8 h to reach 650 °C, temperature which was then kept for 5 h, being subsequently cooled in a two-step process: 50 h at 400 °C followed by at least 25 h at 100 °C. Finally, the ampoule was opened inside a glovebox and washed with dry toluene and carbon disulphide. BP was stored inside the glovebox until further use.

2.3.2. Preparation of modified SPEs

BP suspension was prepared with deoxygenated ultrapure water and sonicated for 30 min at a temperature lower than 20 °C. Unless otherwise specified, BP-SPCE was prepared by drop-casting 5 μL of BP suspension (1.25 mg mL^{-1}) on the carbon working electrode surface and letting the solvent evaporate in the oven at 25 °C for 30 min in the presence of oxygen and air moisture. The BP-SPCE used shortly after preparation is designed as BP-$SPCE_{0d}$.

The BP suspension can be stored for further uses at 0 °C at least for 3 months without signs of degradation or stability loss. Previously to its use, the BP suspension should be defrosted and sonicated for 10 min.

2.3.3. Voltammetric measurements

DA determinations were conducted by differential pulse voltammetry (DPV) at room temperature under the following conditions: potential range from −0.2 V to 0.25 V, modulation time of 50 ms, step potential of 5 mV and modulation amplitude of 100 mV.

For each new sensor unit and before starting the reliable measurements, three scans were done in phosphate buffer (pH = 7) to equilibrate the SPE. A new sensor unit was used for each experiment.

Linear calibration plots for DA were obtained in triplicate by DPV at the above-mentioned conditions by increasing DA concentration from 0.05 to about 4 μM in 0.1 M phosphate buffer (pH = 7).

Urine sample was collected from a healthy volunteer. The collected

sample was spiked with DA and 100-fold diluted in phosphate buffer (pH = 7) to a final concentration of 1.0 μM. The analysis of the urine sample using a BP-SPCE was done in triplicate by the standard addition calibration method. DPV measurements were done following the above established conditions without any additional sample treatment. Moreover, non-spiked urine sample was analyzed to confirm the absence of DA.

3. Results and discussion

3.1. Morphological and chemical characterization of black phosphorus

The 2D layered puckered crystal structure comprising corrugated lamellae of phosphorus atoms held together by weak interlayer forces is shown in Fig. 1A. The chemical structure of BP has a free pair of electrons and a hydrophilic surface that leads to the decomposition of orthorhombic BP to P_xO_y species in the presence of O_2 or H_2O. The BP was synthesized by vapor-grown, yielding nicely defined pellets and layers of mm-wide crystals (Fig. 1B). BP was suspended in aqueous media and drop-casted to a SPCE with a diameter of 4 mm. The BP-SPCE was observed by SEM at low magnification to verify the deposition of the material at the SPCE, as shown in Fig. 1C. EDS mapping of elements shows that the majority of BP is concentrated in a well-defined 1 mm diameter, as shown in Fig. 1C. BP-SPCE was characterized by Raman scattering spectroscopy, which in the range of 300–500 cm^{-1} conveys valuable information about BP as a result of the three distinct peaks corresponding to the A_g^1, B_{2g} and A_g^2 vibrational modes of the phosphorus atoms in BP structure at 364, 440 and 468 cm^{-1}, respectively (Figure S1A). While the B_{2g} and A_g^2 modes correspond to vibrational modes where atoms oscillate within the layer plane, in the A_g^1 mode phosphorus atoms vibrate out-of-plane [26]. In the case of the substrate carbon-based material, Raman spectroscopy is commonly used to measure the degree of bond disorder or $sp^{3/sp2}$ ratio by monitoring the intensity ratio for the D and G bands (I_D/I_G). Figure S1B shows the D band at 1362 cm^{-1} and G band at 1585 cm^{-1} with a I_D/I_G of 1.1, which points to a graphitic material of high structural disorder [27].

3.2. Optimization of the concentration of the BP modifier suspension

Firstly, both background solution and potential range were optimized in relation to the determination of DA as a model target. DPV measurements of 0.3 μM DA were performed in both 0.1 M phosphate buffer at pH = 7 and 0.1 M acetate buffer at pH = 4.5. The characteristic DA peak was only observed in phosphate buffer (pH = 7). Different potential ranges with an initial potential of −0.2 V and an end potential ranging from 0.2 to 0.45 were also studied. After analyzing these results, a potential range from −0.2 V to 0.25 V in 0.1 M phosphate buffer at pH = 7 was established for the experimental work. Once the experimental conditions were set up, the concentration of the BP modifier suspension drop-casted onto the working electrode of the SPCE was optimized. Different concentrations of the BP modifier suspension ranging from 0.75 to 1.5 mg mL^{-1} (Fig. 2) were evaluated at 25 °C for a drying time of 30 min, which is the time necessary for a total and homogeneous drying of the BP suspension dropped onto the SPCE. As observed in Fig. 2, the drop-casting of 5 μL of 1.25 mg mL^{-1} BP suspension onto the carbon electrode surface led to the optimal DA voltammetric response, providing a well-defined peak with the highest current. The obtained voltammetric peak was also higher than that displayed by the bare-SPCE. Thus, for further experiments, BP-SPCE was prepared by using a 1.25 mg mL^{-1} BP modifier suspension.

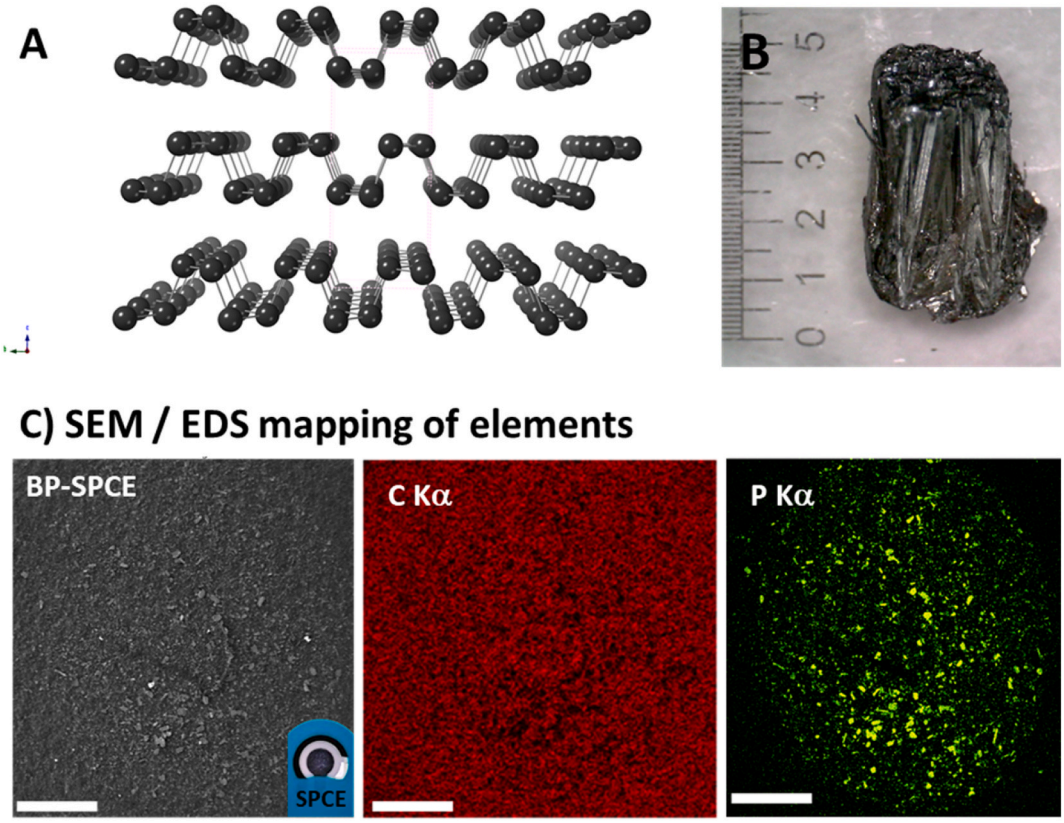

Fig. 1. (A) Side view of the 2D layered orthorhombic BP crystal structure. (B) Representative image of a multi-mm size orthorhombic BP crystal grown by vapor transport (photo credit: F. M. Oliveira). (C) SEM image of BP-SPCE with the respective EDS mapping of C and P. The scale bar represents 0.5 mm. Inset: photo of the 3-electrode configuration of the BP-SPCE.

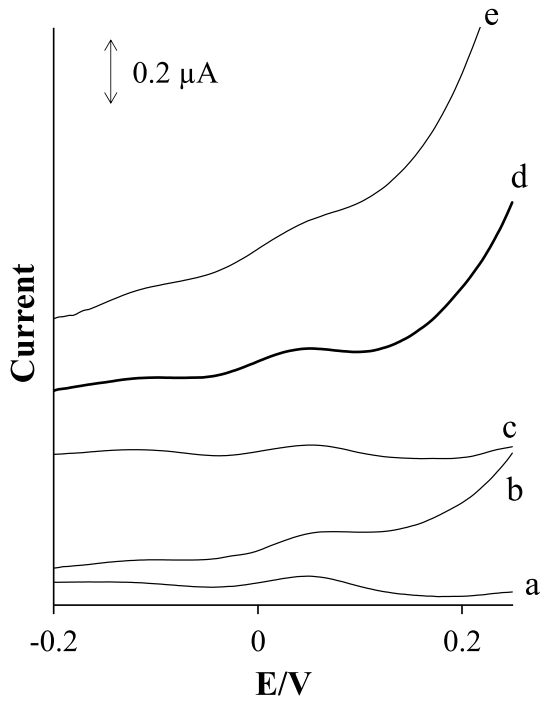

Fig. 2. Differential pulse voltammograms of 1 μM dopamine in 0.1 M phosphate buffer (pH = 7) using a bare-SPCE (a) and BP-SPCE$_{0d}$ at 0.75 (b), 1.0 (c), 1.25 (d), 1.5 (e) mg mL^{-1} BP.

3.3. Stability of BP sensors

As it is pointed out in the introduction section, one of the main drawbacks of working with BP is that it is chemically unstable and tends to be degraded under ambient conditions leading to the formation of oxidized phosphorous species. This BP degradation may result in a decreased analyte response and, therefore, restricts its use for electrochemical sensing applications, making necessary the implementation of strategies seeking to preserve BP intrinsic properties [17–19]. However, as it is also stated in the introduction, some studies have taken advantage of oxidized BP and proposed its use as gas sensor, humidity sensor, to favor BP lubrication behavior or to create exceptional functional optoelectronic capabilities [9,20,21].

Considering this duality of behavior, the voltammetric signal response of BP-SPCE towards DA was studied. For this purpose, BP-SPCE was stored in the oven at 25 °C in the presence of oxygen and air moisture for 15 days and its voltammetric response towards DA was monitored in a daily basis by measuring in triplicate a solution containing 0.8 μM DA in phosphate buffer at pH = 7. Bare-SPCE stored under the same conditions and BP-SPCE stored in the oven under vacuum (i.e. anhydrous conditions) were used for control purposes. As it can be seen in Fig. 3A, whereas the DA peak area using a BP-SPCE stored under vacuum remained practically constant over the 15 days, a gradual increase of the DA peak area was observed when a BP-SPCE stored without vacuum conditions was used. More specifically, the DA peak area progressively increased from day 0 to day 10 and was kept practically constant for the remaining four days, reaching a peak area up to 5-fold higher than that initially measured (day 0). This behavior can be attributed to a faster oxidation of the BP surface during the first days as can be observed in Fig. 3B, where the voltammetric peak associated to the oxidation of BP at 0.3 V gradually decreases over time, with a faster decrease in the first three days. No noticeable changes in the DA peak area were found for the bare-SPCE, confirming that the signal increase is related to the presence of BP. Fig. 3C shows the DP voltammograms of 0.8 μM DA obtained using a bare-SPCE and BP-SPCEs stored without vacuum for a different number of days (BP-SPCE$_{0d}$, BP-SPCE$_{5d}$, BP-SPCE$_{10d}$ and BP-SPCE$_{14d}$). As compared to bare-SPCE (thin line), the BP-SPCE$_{0d}$ (dotted thin line) slightly increased the voltammetric response for DA, whereas a substantial enhancement of the voltammetric response was observed for BP-SPCE$_{5d}$ (dashed thin line). This enhancement was much more remarkable for both BP-SPCE$_{10d}$ (thick line) and BP-SPCE$_{14d}$ (dashed thick line), which presented a similar voltammetric response.

The peak area enhancement observed only in the case of BP-SPCE stored without vacuum conditions points out BP oxidation in the presence of oxygen and humidity as a key factor in the improved voltammetric sensing of DA, validating our initial assumption that oxidized BP could be advantageous for electrochemical sensing applications.

In order to make logic of the verified electrochemical sensing results, BP-SPCEs at different conditioning days were characterized by SEM-EDS, Raman, and XPS. Fig. 4A and B shows the SEM micrograph layered with the mapping of C, O and P signals with the respective EDS spectra recalculated from the areas corresponding to higher BP flakes presence. In the EDS spectra it was observed an increment of O peak at *ca.* 0.5 keV along with the number of days (Fig. 4B). Although there was no significant change in the shape and angles of the BP flakes, for BP-SPCE$_{14d}$ at higher magnifications it was observed what can be described as humidity blobs at the edges of the BP flakes (Figures S2A and B). This is a sign of oxidation of BP which was observed to be more noticeable at the edges of the flakes, which has also been described by other authors [28,29]. Signals assigned to P element were observed at 0.1, 2.0 and 2.1 keV (shown in Fig. 4B). P/O atomic percentage ratio, calculated from the spectra signals, decreased from an initial value of 26 to 7, indicating a much higher presence of oxygen for BP-SPCE$_{14d}$ (Fig. 4B and S3A). It is also interesting to note in Fig. 4A and S2C that the mapping of O element changes from being low intensity, but evenly distributed in BP-SPCE$_{0d}$ to coinciding and well defining the shapes and edges of BP crystal for BP-SPCE$_{14d}$.

Raman spectroscopic measurements were conducted on the BP flakes to identify the produced chemical groups during air degradation. Fig. 5A shows the Raman scattering spectra of the initial BP-SPCE$_{0d}$ and exposed to the ambient conditions for 5, 11 and 14 days, within Raman shift of 300–500 cm^{-1}.

The three characteristic BP peaks were observed in all samples, indicating the persistence of the BP flakes after electrochemical sensing [30]. It has been shown that the intensity ratio of the A_g^1/A_g^2 phonon sensitively depends on sample degradation [13]. The spectra of the different BP-SPCE all registered a $A_g^1/A_g^2 > 0.6$. Relatively smaller and broad peaks composed of several Raman modes were observed for the 700−1000 cm^{-1} range for the degraded BP flakes (Fig. 5B). More importantly, the peaks located at 800−900 cm^{-1}, which is referred to the second-order spectrum of BP [20], became predominant as BP flakes were exposed to the air for longer times.

According to the reported Raman shifts that are related to various P–O functional groupsets, it can be assumed that the peaks within the 800−900 cm^{-1} range are mainly assigned to the Raman active modes of P_xO_y [31]. No peaks were observed for the starting BP and after 5 days. However, when exposed to ambient conditions for 11–14 days, these peaks became predominant. This is due to the exposed layer of BP flakes becoming composed of P═O and P–O–P bonds and owing to the oxidized phosphorus as well as possible $P(OH)_3$ groups, considering water absorption.

XPS is a much more surface-sensitive technique than EDS and was thus employed to characterize BP surfaces at SPCE surface. The chemical bonding characteristics of the BP$_{xd}$ were also investigated by the high-resolution XPS spectrum (Fig. 5C). The P 2p core level has closely spaced spin-orbit components (Δ~0.9 eV), with the signals corresponding to P $2p_{3/2}$ and P $2p_{1/2}$ detected at 128.8 and 129.7 eV, respectively, for elemental P–P bonding [13,32]. A broad peak centered at *ca.* 134–136 eV is attributed to P–O bonds, as a consequence of BP oxidation, usually assigned to clusters of P_xO_y species. As shown in

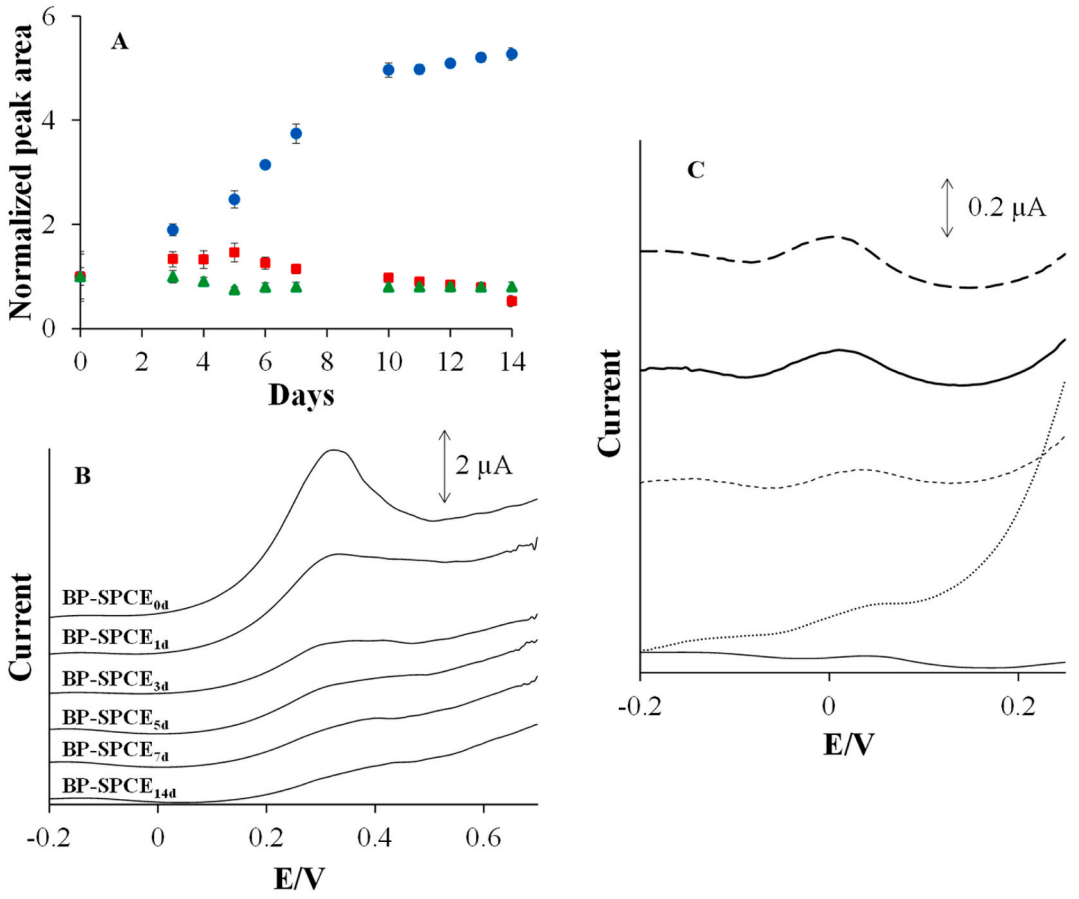

Fig. 3. (A) Effect of storing days on the peak area of dopamine signal using a BP-SPCE (●) and bare-SPCE (▲) stored in the oven at 25 °C without vacuum conditions, and BP-SPCE stored under vacuum conditions (■). Experimental conditions: pH = 7; C_{DA} = 0.8 μM. Error bars of the peak areas are shown. (B) Inherent electrochemistry of BP-SPCE stored in the oven for a different number of days at 25 °C without vacuum conditions. Differential pulse voltammograms were recorded in 0.1 M phosphate buffer (pH = 7) starting at −0.2 V (*vs* Ag/AgCl/KCl (3 M) reference electrode) in the anodic direction. (C) Differential pulse voltammograms of 0.8 μM dopamine in 0.1 M phosphate buffer (pH = 7) using a bare-SPCE (thin line) and BP-SPCEs stored without vacuum condition for different days: $BP\text{-}SPCE_{0d}$ (dotted thin line), $BP\text{-}SPCE_{5d}$ (dashed thin line), $BP\text{-}SPCE_{10d}$ (thick line), and $BP\text{-}SPCE_{14d}$ (dashed thick line).

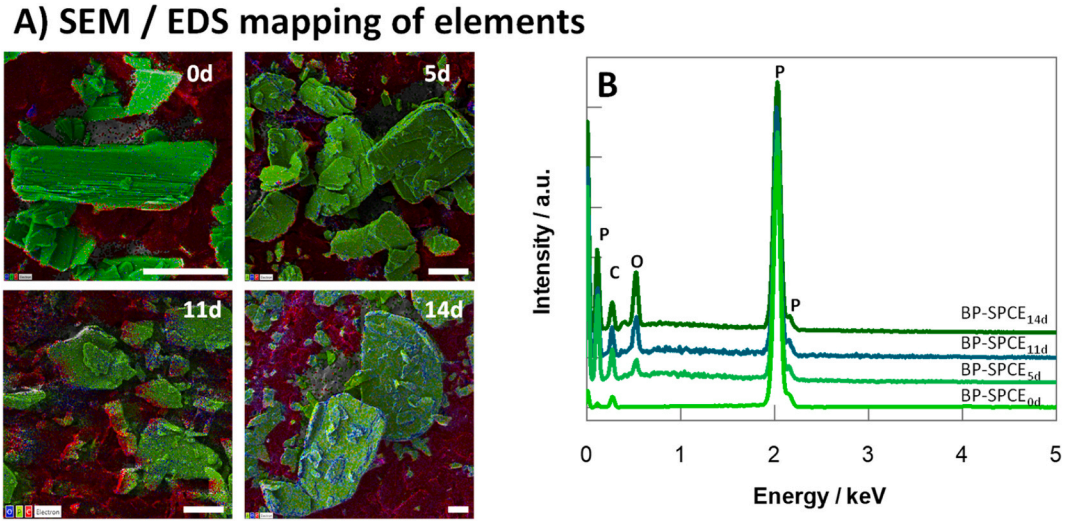

Fig. 4. SEM image of BP-SPCE at different usage days, overplayed with the EDS mapping of elements for C in red, O in blue and P in green (A). The scale bar represents 10 μm. (B) Respective EDS spectra. (For interpretation of the references to colour in this figure legend, the reader is referred to the Web version of this article.)

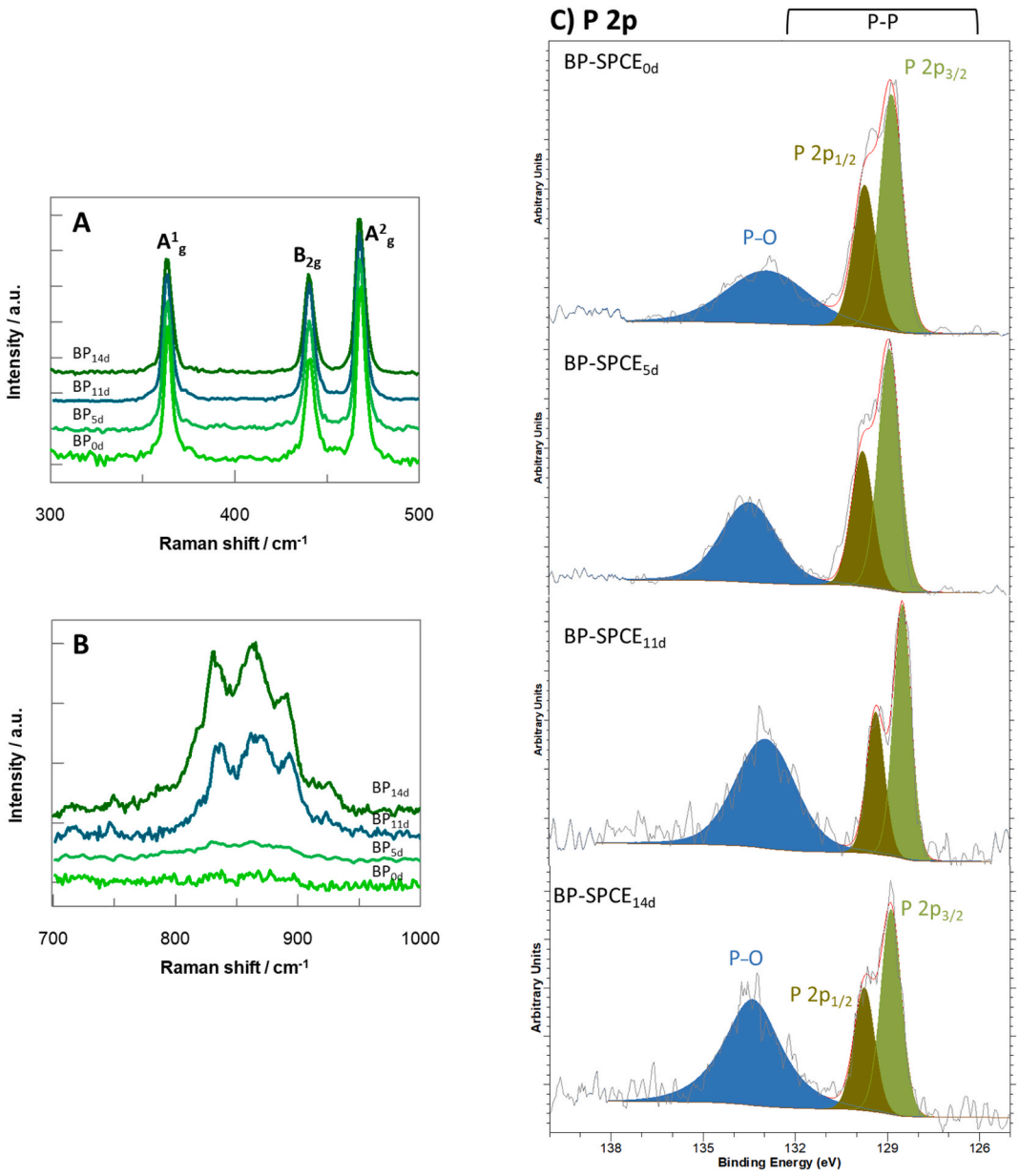

Fig. 5. Raman and XPS spectra of BP-SPCE exposed in ambient conditions at different days: (A) Raman characteristic peaks within the range of 300–500 cm^{-1}. (B) Raman spectra within the range of 700–1000 cm^{-1}. (C) XPS spectra and peaks deconvolution for the P 2p region.

Figure S3B, this component increases considerably starting at *ca.* 20% BP_{0d} and stabilizing *ca.* 35% for BP_{14d}, thus confirming data from Raman and EDS. It has been proposed that outer oxidized BP layers can act as a native capping layer, leaving core BP layers intact [33].

It is therefore clear that this remarkable enhancement of the BP-SPCE response towards DA could be attributed to the interaction between DA and oxidized BP. In particular, we hypothesize that this interaction is facilitated through electrostatic interactions between the positively charged DA and the high electron density on the surface of oxidized BP.

In fact, DA is a polyprotic molecule with a basic amino and two potentially acidic phenolic hydroxyl groups. The ACD/Labs software [34] allows to easily calculate these pK_a values, but sensibly different results are obtained depending on the module used: 10.1 ± 0.1, 9.4 ± 0.3, and 12.7 ± 0.2, respectively, for the Classic algorithm, but 8.6 ± 0.4, 10.5 ± 0.4 and 14.3 ± 0.4 according to the GALAS one. Both modules point out that the acidic character of the second phenolic group (after deprotonation of the first one) is extremely weak, but the Classic algorithm indicates that the most acidic pK_a corresponds to a phenolic group, whereas the Galas module refers to the protonated amino as the most acidic functional group in the molecule. Fortunately, the acidity constants of DA were potentiometrically determined at 25 °C by Mack and Bönisch [35], and the reported pK_a values for the amino and the first phenolic group are 8.88 and 10.39, respectively, confirming the estimation provided by the GALAS module. This means that at the working pH of 7 the molar fraction of the fully protonated (and thus positively charged) DA is about 99%.

Different structural models for the oxidation of BP are proposed depending on the degree of exposure to O_2, with phosphorous atoms that have between 1 and 4 neighboring oxygens, including surface dangling P═O bonds and oxygen bridging (P–O–P), and interstitial P–O–P bonds. At the end of the oxidation process the surface layer of BP is thought to be saturated by incomplete P_2O_5, which is the most stable molecular form of phosphorus oxides and forms phosphoric in the presence of water [36]. The presence of oxygen atoms on the surface of oxidized BP, or even negatively charged species from deprotonated phosphoric, might lead to a surface of high electron density prone to reactivity with

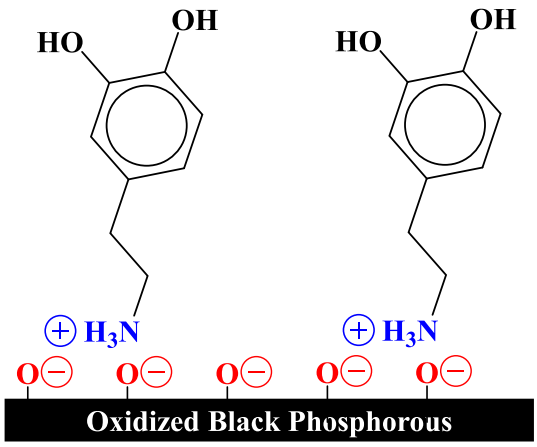

Fig. 6. Schematic representation of electrostatic interactions between the positively charged DA at pH = 7 and oxidized BP with a high electron density on its surface.

DA (Fig. 6). Indeed, interactions between BP and amino groups have already been reported by Su et al. [37] in their study on the improvement of BP stability by coating its surface with an alkylamine monolayer through P–O^-–NH_3^+–R bindings.

In order to confirm that the affinity between DA and BP-SPCE is facilitated through electrostatic interactions between the positively charged target analyte and the high electron density on the surface of oxidized BP, the electrochemical response also at pH = 7 of epinephrine (positively charged) and ascorbic acid (negatively charged) was evaluated using BP-$SPCE_{0d}$ and BP-$SPCE_{10d}$. As it is shown in Figure S4A, epinephrine signal recorded using BP-$SPCE_{10d}$ was about 1.6-fold higher than that provided by BP-$SPCE_{0d}$, thus presenting an analogous behavior to DA, also positively charged. On the contrary, the negatively charged ascorbic acid shows the opposite behavior, with a 1.3-fold decrease of the voltammetric signal when using BP-$SPCE_{10d}$ (Figure S4B).

At the view of these results, in order to favor DA determination, BP-SPCE should be used after being stored for at least 10 days in the oven at 25 °C without vacuum conditions. On the other hand, the sustained BP-SPCE response observed from day 10 to day 14 indicates that once BP is oxidized, the BP-SPCE has a good stability (RSD = 2.7%) for at least four days more.

3.4. Analytical characterization

Considering the performed study regarding the use of oxidized BP in voltammetric sensors, and to assess if there is an improvement in the analytical performance itself and not only an occasional increase in the peak area of the DA signal, BP-SPCE sensors were analytically characterized. At the above-established experimental conditions, the repeatability and reproducibility of the bare-SPCE and BP-SPCEs stored in the oven at 25 °C without vacuum condition for a different number of days (BP-$SPCE_{0d}$, BP-$SPCE_{5d}$, BP-$SPCE_{10d}$ and BP-$SPCE_{14d}$) were assessed (Table 1). Repeatability was estimated using the same bare-SCPE or BP-SPCE sensor for five successive DPV measurements carried out in a solution containing 0.8 μM DA in phosphate buffer at pH = 7. Similar repeatability values with a RSD (%) close to 1% were obtained for both bare-SPCE and BP-SPCE sensors, demonstrating the good repeatability response of the developed BP sensors. Reproducibility was computed considering the response signal of three different sensor units obtained from three independent measurements of 0.8 μM DA solution under the same conditions. The reproducibility achieved by the BP-$SPCE_{10d}$ and BP-$SPCE_{14d}$ were similar or slightly better than that obtained by the bare-SPCE sensor. In contrast, the reproducibility values found by BP-$SPCE_{0d}$ and BP-$SPCE_{5d}$ were much worse than those achieved by both bare-SPCE and BP-SPCEs stored at least 10 days in the oven at 25 °C without vacuum conditions. This improvement in the reproducibility with respect to the storage time could be associated to the formation, after 10 days at the above-mentioned conditions, of a stable black phosphorus oxide layer [38].

Calibration measurements by DPV were performed by recording increasing concentrations of DA with a bare-SPCE and BP-SPCEs stored for a different number of days (BP-$SPCE_{0d}$, BP-$SPCE_{5d}$, BP-$SPCE_{10d}$ and BP-$SPCE_{14d}$) in order to compare the analytical performance of bare-SPCE and BP-SPCEs as well as to evaluate the effect of BP oxidation on the analytical performance of the BP-SPCE sensors. DPV calibrations were done in triplicate using a new sensor unit in each replicate. A well-defined DA voltammetric oxidation signal, very similar to those shown in Fig. 3C, which increased with DA concentration was obtained for all tested sensors (Figure not shown). The achieved calibration data are reported in Table 1. All tested sensors exhibited excellent linearity for DA until a concentration close to 4 μM, depending on the considered sensor. The sensitivities (nA V μM^{-1}), stated from the slopes of the calibration curves, were in agreement with the peak area enhancement observed for different number of storing days. On the one hand, the sensitivities obtained for all considered BP-SPCEs were higher than that provided by bare-SPCE and, on the other hand, the sensitivity values of BP-SPCEs increased during the first 10 days and stabilized after that. More specifically, BP-$SPCE_{10d}$ and BP-$SPCE_{14d}$ showed a similar sensitivity, which was about 5-fold higher than that presented by bare-SPCE and a little more than 2-fold superior to that achieved by BP-$SPCE_{0d}$. The limit of detection (LOD) and the limit of quantification (LOQ) were determined as 3 and 10 times, respectively, the intercept's standard deviation over the calibration curve's slope. The obtained LODs for both bare-SPCE and BP-SPCEs were all bellow 50 nM. The BP-$SPCE_{0d}$ presented LOD and LOQ values about 1.3-fold higher than those provided by bare-SPCE and, in turn, BP-SPCE sensors stored for some time (from 5 days onwards) showed better LODs and LOQs than BP-$SPCE_{0d}$.

As compared to different sensors reported in the literature for DA determination and summarized in Table 2, the developed BP-SPCEs stored for at least 10 days in the oven at 25 °C without vacuum conditions own, in general, much lower LODs. Moreover, BP-$SPCE_{10d}$ and BP-$SPCE_{14d}$ own a wider linear range than that reported for the majority of the few sensors with lower LODs. Finally, it should be pointed out that the proposed BP-SPCE is a one-step preparation sensor, easy to produce and with a low-cost as compared to other multiple-step preparation and

Table 1
Analytical performance of bare-SPCE and BP-SPCEs stored without vacuum for a different number of days (BP-$SPCE_{0d}$, BP-$SPCE_{5d}$, BP-$SPCE_{10d}$, and BP-$SPCE_{14d}$) for the DPV determination of dopamine in phosphate buffer (pH = 7). The standard deviations are shown within brackets.

	Bare-SPCE	BP-$SPCE_{0d}$	BP-$SPCE_{5d}$	BP-$SPCE_{10d}$	BP-$SPCE_{14d}$
Sensitivity (nA V μM^{-1})	4.31 (0.04)	10.09 (0.06)	16.75 (0.08)	22.75 (0.08)	21.16 (0.08)
Intercept (μM)	−0.52 (0.05)	−3.40 (0.09)	−4.5 (0.1)	−4.4 (0.2)	−3.3 (0.1)
R^2	0.997	0.999	0.999	0.999	0.999
Linear range (μM)[a]	0.12–3.45	0.09–3.45	0.08–3.67	0.07–4.16	0.07–4.16
LOD (μM)	0.04	0.03	0.02	0.02	0.02
Repeatability (at 0.8 μM, n = 5, %)	1.2	1.4	1.2	0.9	1.1
Reproducibility (at 0.8 μM, n = 3, %)	3.3	5.8	5.5	3.2	2.5

[a] The lowest level of the linear range was established from the LOQ.

Table 2
Summary of various reported sensors for the determination of dopamine.

Electrode	Technique	Linear range (μM)	LOD (μM)	Application	Ref.
GCE/IL/PEDOT	CV,I-T	0.2–328	0.033	Human urine	[39]
Au/HBMs	SWV	1×10^{-6}-$8 \times 10^{\wedge-5}$	4.1×10^{-7}	–	[40]
GF/Au NPs/ZnO nanocone arrays	DPV	0–80	0.04	Human urine	[41]
GCE/PFSG	DPV	0.002–2	0.0008	Human serum	[42]
Co–Ni/GCE	CV, DPV	10–500	8.2	–	[43]
Pt–Ni/rGO/GCE	DPV	0.01–100	0.0026	Human blood, pharmaceutical formulations	[44]
Cu/Cu_xO/PGEs	DPV	0.3–53	1.07	–	[45]
CDP-Choline/MCPE	DPV	10–100	3.96	Pharmaceutical sample	[46]
GCE/MWCNT/CAP	CA	5–115	1.80	Pharmaceutical sample	[47]
PXa/Au/Cu-TCPP/GCE	DPV	5–125	1.0	Human serum	[48]
2D-MoS_2-SPCE	LSV	1–100	0.085	–	[49]
Ti–C-T_x/GCE	DPV	0.5–50	0.06	Human urine	[50]
Siloxene/GCE	DPV	10-190; 200–1100	0.327	–	[51]
ZnS/Nb_2C/GCE	DPV	820–90	1.39	–	[52]
BP-$SPCE_{10d}$ BP-$SPCE_{14d}$	DPV	0.07–4.16	0.02	Human urine	This work

2D-MoS_2: two-dimensional molybdenum disulphide nanosheets; CA: chronoamperometry; CAP: capsaicin; CDP-Choline: cytidinediphosphate-choline; Cu-TCPP: Cu-tetrakis(4-carboxyphenyl)porphyrin; CV: cyclic voltammetry; DPV: differential pulse voltammetry; GCE: glassy carbon electrode; GF: graphene foam; HBMs: hybrid bilayer membranes; IL: ionic liquid; NPs: nanoparticles; LSV: linear sweep voltammetry; MCPE: modified carbon paste electrode; MWCNT: multiwalled-carbon nanotubes; PEDOT: poly(3,4-ethylenedioxythiophene); PFSG: poly(sodyum 4-styrenesulfonate)-functionalized three dimensional graphene; PGEs: pencil graphite electrodes; PXa: poly(xanthurenic acid); rGO: reduced graphene oxide; SPCE: screen-printed carbon electrode; SWV: square wave voltammetry; Ti–C-T_x: titanium carbide MXene (T_x = –F, –OH, or –O).

more expensive sensors. Moreover, BP-SPCEs take advantage of the inherent features of SPEs, for example, they are disposable and accessible supports that do not require to be polished before each analysis.

Regarding BP-SPCE selectivity, it was assessed by the analysis of common interfering reagents such as ascorbic acid, uric acid, salicylic acid, paracetamol, epinephrine, serotonin, and ibuprofen. These substances were independently added to a solution containing 0.8 μM DA in phosphate buffer (pH = 7) at DA:reagent ratios of 1:0.01, 1:0.02, 1:0.1, 1:0.2, 1:1, 1:5, 1:10, 1:50 and 1:100, and the voltammetric response was recorded using BP-$SPCE_{0d}$ and BP-$SPCE_{10d}$. The addition of ascorbic acid, epinephrine, and serotonin resulted in a significant variation of the DA voltammetric signal. Specifically, the DA voltammetric signal increased with the addition, even at lower ratios, of ascorbic acid and epinephrine due to the similar oxidation potential [53]. In contrast, the addition of serotonin at DA:serotonin ratios equal or higher than 1:1 gave rise to a considerable decrease of the DA voltammetric signal due to the competitive adsorption of DA and serotonin, both positively charged at pH 7, at the BP-SPCE sensor [54]. It should be noted that these interfering effects in the DA response signal were similar for both tested BP-SPCEs, although somewhat more accentuated in the case of BP-$SPCE_{10d}$. Other substances, whose oxidation potentials were apparently distinct from that of DA, did not seem to affect the determination of DA.

Hence, the analytical features of BP-SPCEs are not only better than those of bare-SPCE but also the exposure of the BP-SPCE sensor to the oxygen and moisture for some days, which in many works would be considered as serious impediment for its application in ambient conditions, has been shown to lead to a noticeable improvement of its analytical performance. This suggests that the use of a BP-SPCE stored for at least 10 days in the oven at 25 °C without vacuum conditions would be an excellent option for the determination of DA due to the remarkable features that oxidized BP provides to the sensor.

3.5. Real sample analysis

In order to corroborate the applicability of the oxidized BP modified SPCE, the determination of DA in human urine samples spiked with 1.0 μM of DA was performed by the standard addition calibration method. DPV measurements of the spiked urine sample at the above established conditions using BP-$SPCE_{10d}$ were carried out, together with four consecutive additions of DA solution. It should be noted that DPV measurements of non-spiked urine samples on BP-$SPCE_{10d}$ did not show any DA signal.

Fig. 7A displays representative DP voltammograms obtained for the determination of the spiked urine sample using BP-$SPCE_{10d}$. A well-defined DA peak was attained and the DA calibration curves (Fig. 7B) showed a good correlation.

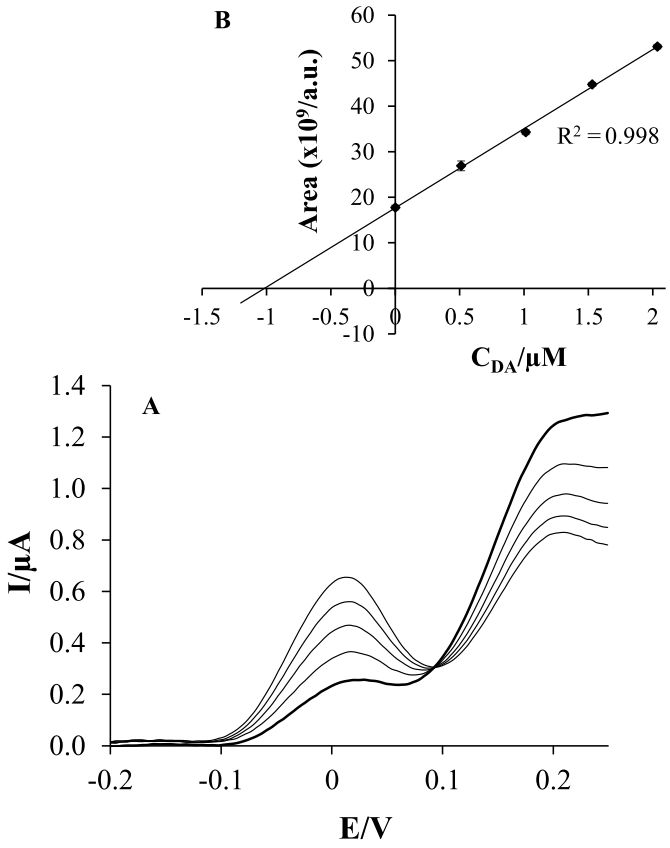

Fig. 7. (A) Differential pulse voltammograms of dopamine in a urine sample using a BP-$SPCE_{10d}$ in 0.1 M phosphate buffer (pH = 7); (B) Dopamine standard addition calibration plot. In (B) error bars of the peak areas are shown.

The analysis of the spiked urine sample on BP-SPCE$_{10d}$ was done in triplicate, using a new BP-SPCE$_{10d}$ unit in each replicate. The result of the analysis was 1.02 μM (SD: 0.03 μM) with a recovery of 101.5%.

These remarkable results verify the appropriateness of BP-SPCE$_{10d}$ for the DPV determination of DA in biological samples. Therefore, the use of oxidized BP modified SPCE is an excellent option to other sensors for the determination of DA at very low μM concentrations in ambient conditions.

4. Conclusions

In this work, the enhancement of voltammetric sensitivity using an oxidized BP-SPCE was demonstrated for the first time with DA as a model target analyte. Characterization points to high content of P_xO_y at the BP surface that stabilizes at *ca.* 35% after 14 days of usage and, the EDS mapping of elements indicates a high O content located at the edges of BP flakes. After aging BP-SPCE for at least 10 days under ambient conditions, the extensive oxidation of the surface of BP drop-casted onto the SPCE takes place, favoring at the working conditions the electrostatic interaction between positively charged DA and the high electron density on BP surface. The proposed oxidized BP-SPCE sensor presented an enhanced sensitivity of 5-fold and 2-fold as compared to bare-SPCE and BP-SPCE stored in anhydrous atmosphere, respectively. In addition, oxidized BP-SPCE was able to detect DA with a detection limit of 0.02 μM, and good repeatability, reproducibility, stability, and selectivity were also achieved. Finally, the suitability of oxidized BP-SPCE for the analysis of biological samples was assessed by the successful determination of DA in spiked urine samples with a very high reproducibility and good recoveries.

Thus, these exceptional features allow us to conclude that oxidized BP-SPCE sensor is not only better than bare-SPCE but also than BP-SPCE stored in anhydrous atmosphere for dopamine electrochemical sensing as well as for other electrochemical active compounds positively charged at the working pH. Moreover, the intrinsic advantages of the SPEs as a support, *i.e.*, disposability, low-cost, commercially availability, and the non-need of previous polishing before the BP attachment, contribute to add value to the developed BP sensor.

Taking into account the chemical and electrostatic nature of the modification produced in layered BP by the oxidation process, we believe that the enhancement of the sensing power is not exclusive of DA. On the contrary, it could be extensive to many other polar or ionizable substances, a point that should be carefully investigated.

This work opens up many possibilities for studying the performance of BP based-sensors for electrochemical sensing at ambient conditions.

Credit author statement

María A. Tapia: Methodology; Formal analysis; Investigation; Visualization, Rui Gusmão: Conceptualization; Methodology; Formal analysis; Writing - original draft; Visualization; Supervision; Resources, Clara Pérez-Ràfols: Methodology; Writing - review & editing; Visualization, Xavier Subirats: Methodology; Writing - review & editing; Visualization, Núria Serrano: Conceptualization; Methodology; Formal analysis; Writing - original draft; Visualization; Supervision; Resources, Zdeněk Sofer: Methodology; Writing - review & editing; Visualization; Resources, José Manuel Díaz-Cruz: Methodology; Formal analysis; Validation; Writing - review & editing; Visualization; Resources.

Declaration of competing interest

The authors declare that they have no known competing financial interests or personal relationships that could have appeared to influence the work reported in this paper.

Acknowledgments

This work is supported by the Ministry of Science and Innovation of Spain (Project PID2019-107102RB-C22) and the Generalitat of Catalunya (Project 2017SGR311). M.A.T. would like to thank the Peruvian National Program of Scholarships and Student Loans (PRONABEC) for her Ph.D grant (Beca Presidente de la República – 343245). M.A.T. appreciates the support of the Water Research Institute (IdRA) of the University of Barcelona. Financial support from the Czech Science Foundation (Project GACR No 19-26910X) is also gratefully acknowledged.

Appendix A. Supplementary data

Supplementary data to this article can be found online at https://doi.org/10.1016/j.talanta.2021.123036.

References

[1] A.K. Geim, K.S. Novoselov, The rise of graphene, Nat. Mater. 6 (2007) 183–191, https://doi.org/10.1038/nmat1849.
[2] K.S. Novoselov, A.K. Geim, S.V. Morozov, D. Jiang, Y. Zhang, S.V. Dubonos, I. V. Grigorieva, A.A. Firsov, Electric field effect in atomically thin carbon films, Science 306 (2004) 666–669, https://doi.org/10.1126/science.1102896.
[3] X. Ge, Z. Xia, S. Guo, Recent advances on black phosphorus for biomedicine and biosensing, Adv. Funct. Mater. 29 (2019) 1900318, https://doi.org/10.1002/adfm.201900318.
[4] A. Gupta, T. Sakthivel, S. Seal, Recent development in 2D materials beyond graphene, Prog. Mater. Sci. 73 (2015) 44–126, https://doi.org/10.1016/j.pmatsci.2015.02.002.
[5] M.A. Tapia, R. Gusmão, N. Serrano, Z. Sofer, C. Ariño, J.M. Díaz-Cruz, M. Esteban, Phosphorene and other layered pnictogens as a new source of 2D materials for electrochemical sensors, TrAC Trends Anal. Chem. 139 (2021) 116249, https://doi.org/10.1016/j.trac.2021.116249.
[6] M.A. Tapia, C. Pérez-Ràfols, R. Gusmão, N. Serrano, Z. Sofer, J.M. Díaz-Cruz, Enhanced voltammetric determination of metal ions by using a bismuthene-modified screen-printed electrode, Electrochim. Acta 362 (2020) 137144, https://doi.org/10.1016/j.electacta.2020.137144.
[7] C.R. Ryder, J.D. Wood, S.A. Wells, M.C. Hersam, Chemically tailoring semiconducting two-dimensional transition metal dichalcogenides and black phosphorus, ACS Nano 10 (2016) 3900–3917, https://doi.org/10.1021/acsnano.6b01091.
[8] S. Kuriakose, T. Ahmed, S. Balendhran, V. Bansal, S. Sriram, M. Bhaskaran, S. Walia, Black phosphorus: ambient degradation and strategies for protection, 2D Mater. 5 (2018), 032001, https://doi.org/10.1088/2053-1583/aab810.
[9] R. Gusmão, Z. Sofer, M. Pumera, Black phosphorus rediscovered: from bulk material to monolayers, Angew. Chem. Int. Ed. 56 (2017) 8052–8072, https://doi.org/10.1002/anie.201610512.
[10] A. Castellanos-Gomez, Black phosphorus: narrow gap, wide applications, J. Phys. Chem. Lett. 6 (2015) 4280–4291, https://doi.org/10.1021/acs.jpclett.5b01686.
[11] S. Zhang, S. Guo, Z. Chen, Y. Wang, H. Gao, J. Gómez-Herrero, P. Ares, F. Zamora, Z. Zhu, H. Zeng, Recent progress in 2D group-VA semiconductors: from theory to experiment, Chem. Soc. Rev. 47 (2018) 982–1021, https://doi.org/10.1039/c7cs00125h.
[12] T. Ahmed, S. Balendhran, N. Karim, E.L.H. Mayes, M.R. Field, R. Ramanathan, M. Singh, V. Bansal, S. Sriram, M. Bhaskaran, S. Walia, Degradation of black phosphorus is contingent on UV – blue light exposure, Npj 2D Mater. Appl. 1 (2017) 18, https://doi.org/10.1038/s41699-017-0023-5.
[13] A. Favron, E. Gaufrès, F. Fossard, A.L. Phaneuf-Laheureux, N.Y.W. Tang, P. L. Lévesque, A. Loiseau, R. Leonelli, S. Francoeur, R. Martel, Photooxidation and quantum confinement effects in exfoliated black phosphorus, Nat. Mater. 14 (2015) 826–832, https://doi.org/10.1038/nmat4299.
[14] S. Walia, Y. Sabri, T. Ahmed, M.R. Field, R. Ramanathan, A. Arash, Defining the role of humidity in the ambient degradation of few-layer black phosphorus, 2D Mater. 4 (2017), 015025, https://doi.org/10.1088/2053-1583/4/1/015025.
[15] G. Wang, W.J. Slough, R. Pandey, S.P. Karna, Degradation of phosphorene in air: understanding at atomic level, 2D Mater. 3 (2016), 025011, https://doi.org/10.1088/2053-1583/3/2/025011.
[16] J.D. Wood, S.A. Wells, D. Jariwala, K. Chen, E. Cho, V.K. Sangwan, X. Liu, L. J. Lauhon, T.J. Marks, M.C. Hersam, Effective passivation of exfoliated black phosphorus transistors against ambient degradation, Nano Lett. 14 (2014) 6964–6970, https://doi.org/10.1021/nl5032293.
[17] J. Yoon, Z. Lee, Effective passivation of black phosphorus under ambient conditions, Appl. Microsc. 47 (2017) 176–186, https://doi.org/10.9729/am.2017.47.3.176.
[18] J. Miao, L. Cai, S. Zhang, J. Nah, J. Yeom, C. Wang, Air-stable humidity sensor using few-layer black phosphorus, ACS Appl. Mater. Interfaces 9 (2017) 10019–10026, https://doi.org/10.1021/acsami.7b01833.
[19] W. Yuan, Y. Tang, K. Yang, Z. Hua, F. Yin, D. Xia, Gas sensing investigation on anthraquinone nanowire decorated phosphorene: enhanced stability in

conjunction with superior sensitivity, Chem. Eng. J. 394 (2020) 124933, https://doi.org/10.1016/j.cej.2020.124933.
[20] S. Wu, F. He, G. Xie, Z. Bian, J. Luo, S. Wen, Black Phosphorus: degradation favors lubrication, Nano Lett. 18 (2018) 5618–5627, https://doi.org/10.1021/acs.nanolett.8b02092.
[21] T. Ahmed, S. Kuriakose, S. Abbas, M.J.S. Spencer, M.A. Rahman, M. Tahir, Y. Lu, P. Sonar, V. Bansal, M. Bhaskaran, S. Sriram, S. Walia, Multifunctional optoelectronics via harnessing defects in layered black phosphorus, Adv. Funct. Mater. 29 (2019) 1901991, https://doi.org/10.1002/adfm.201901991.
[22] Y. Shao, J. Wang, H. Wu, J. Liu, I.A. Aksay, Y. Lin, Graphene based electrochemical sensors and biosensors: a review, Electroanalysis 22 (2010) 1027–1036, https://doi.org/10.1002/elan.200900571.
[23] H. Beitollai, M. Safaei, S. Tajik, Application of graphene and graphene oxide for modification of electrochemical sensors and biosensors: a review, Int. J. Nano Dimens. (IJND) 10 (2019) 125–140, https://doi.org/10.1016/j.trac.2015.07.008.
[24] M.O. Klein, D.S. Battagello, A.R. Cardoso, D.N. Hauser, J.C. Bittencourt, R. G. Correa, Dopamine: functions, signaling, and association with neurological diseases, Cell. Mol. Neurobiol. 39 (2019) 31–59, https://doi.org/10.1007/s10571-018-0632-3.
[25] S.K. Arumugasamy, G. Chellasamy, S. Gopi, S. Govindaraju, K. Yun, Current advances in the detection of neurotransmitters by nanomaterials : an update, Trends Anal. Chem. 123 (2020) 115766, https://doi.org/10.1016/j.trac.2019.115766.
[26] J. Wu, N. Mao, L. Xie, H. Xu, J. Zhang, Identifying the crystalline orientation of black phosphorus using angle-resolved polarized Raman spectroscopy, Angew. Chem. Int. Ed. 54 (2015) 2366–2369, https://doi.org/10.1002/anie.201410108.
[27] R. Gusmão, V. López-Puente, I. Pastoriza-Santos, J. Pérez-Juste, M.F. Proença, F. Bento, D. Geraldo, M.C. Paiva, E. González-Romero, Enhanced electrochemical sensing of polyphenols by an oxygen-mediated surface, RSC Adv. 5 (2015) 5024–5031, https://doi.org/10.1039/c4ra12660b.
[28] X. Ren, X. Yang, G. Xie, F. He, R. Wang, C. Zhang, D. Guo, J. Luo, Superlubricity under ultrahigh contact pressure enabled by partially oxidized black phosphorus nanosheets, Npj 2D Mater. Appl. 5 (2021) 44, https://doi.org/10.1038/s41699-021-00225-0.
[29] V. Lloret, E. Nuin, M. Kohring, S. Wild, M. Löffler, C. Neiss, M. Krieger, F. Hauke, A. Görling, H.B. Weber, G. Abellán, A. Hirsch, Noncovalent functionalization and passivation of black phosphorus with optimized perylene diimides for hybrid field effect transistors, Adv. Mater. Interfaces 7 (2020) 2001290, https://doi.org/10.1002/admi.202001290.
[30] G. Abellán, C. Neiss, V. Lloret, S. Wild, J.C. Chacón-Torres, K. Werbach, F. Fedi, H. Shiozawa, A. Görling, H. Peterlik, T. Pichler, F. Hauke, A. Hirsch, Exploring the formation of black phosphorus intercalation compounds with alkali metals, Angew. Chem. Int. Ed. 56 (2017) 15267–15273, https://doi.org/10.1002/anie.201707462.
[31] S.J. Gilliam, S.J. Kirkby, C.N. Merrow, D. Zeroka, A. Banerjee, J.O. Jensen, Raman spectroscopy of rhombohedral P4O10, J. Phys. Chem. B 107 (2003) 2892–2896, https://doi.org/10.1021/jp027854l.
[32] J. Kang, J.D. Wood, S.A. Wells, J.H. Lee, X. Liu, K.S. Chen, M.C. Hersam, Solvent exfoliation of electronic-grade, two-dimensional black phosphorus, ACS Nano 9 (2015) 3596–3604, https://doi.org/10.1021/acsnano.5b01143.
[33] Q. Zhou, Q. Chen, Y. Tong, J. Wang, Light-induced ambient degradation of few-layer black phosphorus: mechanism and protection, Angew. Chem. Int. Ed. 55 (2016) 11437–11441, https://doi.org/10.1002/anie.201605168.
[34] ACD/Labs, Advanced Chemistry Development, Inc, Toronto, ON, Canada, 2014. www.acdlabs.com.
[35] F. Mack, H. Bönisch, Dissociation constants and lipophilicity of catecholamines and related compounds, Naunyn-Schmiedeberg's Arch. Pharmacol. 310 (1979) 1–9, https://doi.org/10.1007/BF00499868.
[36] K.H. Oh, S.W. Jung, K.S. Kim, Tracing the initial state of surface oxidation in black phosphorus, Appl. Surf. Sci. 504 (2020) 144341, https://doi.org/10.1016/j.apsusc.2019.144341.
[37] C. Su, Z. Yin, Q.B. Yan, Z. Wang, H. Lin, L. Sun, W. Xu, T. Yamada, X. Ji, N. Zettsu, K. Teshima, J.H. Warner, M. Dinca, J. Hu, M. Dong, G. Su, J. Kong, J. Li, Waterproof molecular monolayers stabilize 2D materials, Proc. Natl. Acad. Sci. U. S. A 116 (2019) 20844–20849, https://doi.org/10.1073/pnas.1909500116.
[38] M.T. Edmonds, A. Tadich, A. Carvalho, A. Ziletti, K.M. O'Donnell, S.P. Koenig, D. F. Coker, B. Özyilmaz, A.H.C. Neto, M.S. Fuhrer, Creating a stable oxide at the surface of black phosphorus, ACS Appl. Mater. Interfaces 7 (2015) 14557–14562, https://doi.org/10.1021/acsami.5b01297.
[39] Z. Song, G. Sheng, Y. Cui, M. Li, Z. Song, C. Ding, X. Luo, Low fouling electrochemical sensing in complex biological media by using the ionic liquid-doped conducting polymer PEDOT: application to voltammetric determination of dopamine, Microchim. Acta. 186 (2019) 220, https://doi.org/10.1007/s00604-019-3340-x.
[40] F.T. Patrice, L.J. Zhao, E.K. Fodjo, D.W. Li, K. Qiu, Y.T. Long, Highly sensitive and selective electrochemical detection of dopamine using hybrid bilayer membranes, ChemElectroChem 6 (2019) 634–637, https://doi.org/10.1002/celc.201801367.
[41] H.Y. Yue, H.J. Zhang, S. Huang, X.X. Lu, X. Gao, S.S. Song, Z. Wang, W.Q. Wang, E. H. Guan, Highly sensitive and selective dopamine biosensor using Au nanoparticles-ZnO nanocone arrays/graphene foam electrode, Mater. Sci. Eng. C 108 (2020) 110490, https://doi.org/10.1016/j.msec.2019.110490.
[42] L. Wang, R. Yang, L. Qu, P. de B. Harrington, Electrostatic repulsion strategy for high-sensitive and selective determination of dopamine in the presence of uric acid and ascorbic acid, Talanta 210 (2020) 120626, https://doi.org/10.1016/j.talanta.2019.120626.
[43] C. Yang, X. Sun, C. Zhang, M. Liu, Green synthesis of Co-Ni hollow spheres for its electrochemical detection of dopamine, J. Nanoparticle Res. 22 (2020) 55, https://doi.org/10.1007/s11051-020-4775-z.
[44] Y. Veera Manohara Reddy, B. Sravani, H. Maseed, T. Łuczak, M. Osińska, L. Subramanyamsarma, V.V.S.S. Srikanth, G. Madhavi, Ultrafine Pt-Ni bimetallic nanoparticles anchored on reduced graphene oxide nanocomposites for boosting electrochemical detection of dopamine in biological samples, New J. Chem. 42 (2018) 16891–16901, https://doi.org/10.1039/c8nj03894e.
[45] E. Bahrami, R. Amini, S. Vardak, Electrochemical detection of dopamine via pencil graphite electrodes modified by Cu/CuxO nanoparticles, J. Alloys Compd. 855 (2021) 157292, https://doi.org/10.1016/j.jallcom.2020.157292.
[46] S. Deepa, B.E. Kumara Swamy, K. Vasantakumar Pai, Electrochemical sensing performance of citicoline sodium modified carbon paste electrode for determination of dopamine and serotonin, Mater. Sci. Energy Technol. 3 (2020) 584–592, https://doi.org/10.1016/j.mset.2020.06.001.
[47] L.V. da Silva, N.D. dos Santos, A.K.A. de Almeida, D.D.E.R. dos Santos, A.C. F. Santos, M.C. França, D.J.P. Lima, P.R. Lima, M.O.F. Goulart, A new electrochemical sensor based on oxidized capsaicin/multi-walled carbon nanotubes/glassy carbon electrode for the quantification of dopamine, epinephrine, and xanthurenic, ascorbic and uric acids, J. Electroanal. Chem. 881 (2021) 114919, https://doi.org/10.1016/j.jelechem.2020.114919.
[48] Z. Qiu, T. Yang, R. Gao, G. Jie, W. Hou, An electrochemical ratiometric sensor based on 2D MOF nanosheet/Au/polyxanthurenic acid composite for detection of dopamine, J. Electroanal. Chem. 835 (2019) 123–129, https://doi.org/10.1016/j.jelechem.2019.01.040.
[49] R. Zribi, R. Maalej, R. Gillibert, M.G. Donato, P.G. Gucciardi, S.G. Leonardi, G. Neri, Simultaneous and selective determination of dopamine and tyrosine in the presence of uric acid with 2D-MoS2 nanosheets modified screen-printed carbon electrodes, FlatChem 24 (2020) 100187, https://doi.org/10.1016/j.flatc.2020.100187.
[50] N. Murugan, R. Jerome, M. Preethika, A. Sundaramurthy, A.K. Sundramoorthy, 2D-titanium carbide (MXene) based selective electrochemical sensor for simultaneous detection of ascorbic acid, dopamine and uric acid, J. Mater. Sci. Technol. 72 (2021) 122–131, https://doi.org/10.1016/j.jmst.2020.07.037.
[51] R. Ramachandran, X. Leng, C. Zhao, Z.X. Xu, F. Wang, 2D siloxene sheets: a novel electrochemical sensor for selective dopamine detection, Appl. Mater. Today. 18 (2020) 100477, https://doi.org/10.1016/j.apmt.2019.100477.
[52] N. Arif, S. Gul, M. Sohail, S. Rizwan, M. Iqbal, Synthesis and characterization of layered Nb2C MXene/ZnS nanocomposites for highly selective electrochemical sensing of dopamine, Ceram. Int. 47 (2021) 2388–2396, https://doi.org/10.1016/j.ceramint.2020.09.081.
[53] Q.-J. Gong, H.-X. Han, Y.-D. Wang, C.-Z. Yao, H.-Y. Yang, J.-L. Qiao, An electrochemical sensor for dopamine detection using poly-tryptophan composited graphene on glassy carbon as the electrode, N. Carbon Mater. 35 (2020) 34–41, https://doi.org/10.1016/S1872-5805(20)60473-5.
[54] K. Wu, J. Fei, S. Hu, Simultaneous determination of dopamine and serotonin on a glassy carbon electrode coated with a film of carbon nanotubes, Anal. Biochem. 318 (2003) 100–106, https://doi.org/10.1016/S0003-2697(03)00174-X.